Nuclear Materials and Energy 41 (2024) 101753

Contents lists available at ScienceDirect

Nuclear Materials and Energy

journal homepage: www.elsevier.com/locate/nme

Simulated temperature of a tungsten spot facing large plasma heat loads

J. Moritz [a,*], S. Heuraux [a], M. Lesur [a], E. Gravier [a], F. Brochard [a], L. Marot [b], P. Hiret [b]

[a] Institut Jean Lamour, CNRS - Université de Lorraine, 2 allée André Guinier, Nancy, 54011, France
[b] Department of Physics, University of Basel, Klingelbergstrasse 82, Basel, CH-4056, Switzerland

ARTICLE INFO

Keywords:
Thermionic current
Space-charge-limited regime
Tungsten surface
PIC simulations

ABSTRACT

In fusion devices like ITER, plasma-wall interactions are a significant concern due to the high heat fluxes, often tens of MW/m^2, impacting the first wall. These intense heat fluxes can lead to the formation of hot spots on components facing the plasma, such as tungsten, used in divertor plates and antennas. This results in material erosion and plasma core contamination. Our study investigates the thermal behavior of tungsten surfaces under these conditions using fluid modeling and Particle-In-Cell (PIC) simulations. We examine the effects of thermionic electron emission on the sheath potential and heat transmission. The simulations reveal that thermionic emission can decrease the sheath voltage, increasing the surface temperature due to enhanced heat flux due to electrons. Additionally, we explore how the ratio between the spot size (S) and the surrounding surface length (L_y) influences the surface temperature. We find that a higher L_y/S ratio allows the surface to reach higher temperatures before the system enters the space-charge-limited regime, where thermionic current is maximized and considerably larger than the case where the entire surface is emissive ($L_y = S$).

1. Introduction

The use of tungsten (W) as a plasma facing material in future fusion devices such as ITER has raised the issue of plasma core pollution with high-Z metal which can eventually lead to radiative disruption. There are several sources of contamination of the plasma core with W triggered by plasma-wall interactions, including sputtering, droplet ejection following the local melting of elements facing the plasma such as the W mono-blocks that make up the divertor, or unipolar arcs. While sheath rectification close to ion cyclotron range of frequency antennas for instance can lead to physical sputtering of W [1], misaligned mono-blocks in the divertor can experience temperatures up to the W melting temperature due to heat flux of tens of MWm^{-2} [2,3] and induce droplet ejection. These melting events are associated with strong thermionic emission and a net current passing through the sample and returning to the vessel [4]. Several authors have then investigated the role of sheaths near hot emissive W surfaces during ELM phases [5–7] or use successfully numerical tools such as the MEMOS-U code to investigate the macroscopic melt motion driven by the intense volumetric $\vec{J} \times \vec{B}$ force showing the large implication of thermionic emission [8,9]. The latter is also involved in unipolar arcs arising between the metallic surface and the plasma [10]. These arcs can drive a considerable amount of current of several amperes and are fed by the surface material which is released from it instead of the neutral gas or main plasma. They leave the surface with many micron range craters where the material can be splashed away as droplets [11,12].

Thermionic emission of electrons is then particularly relevant in fusion devices and is well known as altering the energy transmission through the sheath [13]. The decrease in sheath potential can increase the heat flux to the wall, raising the surface temperature T_s and the thermionic current J_s according to the Richardson-Dushman equation:

$$J_s = AT_s^2 \exp\left(-\frac{B_w}{k_b T_s}\right), \tag{1}$$

where A is the Dushman's constant and B_w the electron work function. For tungsten [14], $A = 60 \times 10^4$ Am^{-2} K^{-2} and $B_w = 4.55$ eV.

The accumulation of negative charges near the wall, due to thermionic emission, is what causes the decrease in sheath potential ϕ_s and the increase in heat flux on the surface by the plasma electrons. This leads to an increase in T_s and thus in J_s until equilibrium is eventually reached [15]. This feedback loop is also of great importance when applied to dust in tokamaks because it leads to an enhancement of the dust heating by the plasma and its vaporization [16]. The reduction of the sheath potential cannot continue indefinitely until it vanishes though. At a critical and maximum value of the current $J_s = J_s^*$, the electric field on the surface E_s, which is generally negative to accelerate ions and repel electrons, eventually cancels out. This marks the onset of the space-charge-limited (SCL) regime where the sheath potential is at its minimum ϕ_s^* and the thermionic current is regulated.

In this study, we investigate the behavior of a single spot on a tungsten surface when exposed to a hot plasma with varying temperature and density. In the first part of the paper, we present a fluid

* Corresponding author.
E-mail address: jerome.moritz@univ-lorraine.fr (J. Moritz).

https://doi.org/10.1016/j.nme.2024.101753
Received 16 June 2024; Received in revised form 22 August 2024; Accepted 2 October 2024
Available online 8 October 2024

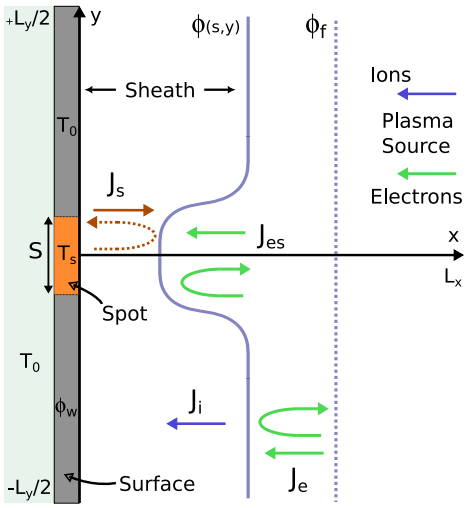

Fig. 1. Sketch of the studied plasma bounded by a grounded conductive wall on its left side. The sheath potential profile $\phi(s,y)$ is indicative of what is expected in 2D, with a slightly lower sheath potential at the vertical of the spot than in the rest of the plasma. The profile of ϕ_f depicted in the figure is indicative of what is expected for the sheath potential in the absence of thermionic emission.

model to evaluate the spot temperature in a 1D approximation. This model accounts for the circulation of electronic current between the spot and the surrounding surface like in the unipolar arc picture [17]. In the second part, 2D Particle-In-Cell (PIC) simulations corroborate the trends deduced from the fluid model and highlight the importance of the ratio between the spot size and the surrounding surface on the maximum thermionic current.

2. Simulated system and fluid model

The simulated system is a hydrogen plasma bounded on one side by a conducting wall that is grounded. On the other side, at $x = L_x$, the electric field is assumed zero. The tungsten surface contains a spot of a fixed size $S = 20$ μm [18], whose thermal conductivity is reduced compared to the surrounding surface of length L_y, as shown in Fig. 1. The spot area could be associated for instance with a point defect induced by He irradiation [19], or it could correspond to a porous redeposit, or even be a dust particle with poor thermal contact with the surface, although in the latter case, it would be preferable to model it through a thermal contact conductance [20]. The spot thermal conductivity κ in our calculations varies between 2.5 and 160 $\mathrm{Wm^{-1}\,K^{-1}}$, but we will mainly focus on a single specific case where $\kappa = 15$ $\mathrm{Wm^{-1}\,K^{-1}}$, which is about 10 times smaller than pristine tungsten.

As a first attempt, we assume that the peripheral surface around the spot has the thermal conductivity of bulk tungsten and remains at temperature T_0 throughout the simulations, which is also the temperature of the cool side of the $l = 1$ cm thick wall as shown in Fig. 1. We arbitrary set this temperature to 300 K, but another operating temperature could be eventually chosen. As a consequence, there is no heat conduction in the y direction nor temperature or thermal conductivity gradients. There is also no magnetic field included in our model, which limits its applicability, as in tokamak plasmas, the magnetic field lines are grazing the surface, and prompt redeposition can completely change the sheath properties with respect to thermionic emission. The latter approximations need to be improved in future studies.

The objective of the present simple model and simulations is to self-consistently calculate the spot temperature T_s as a function of hydrogen plasma parameters (temperature and density), the spot's thermal conductivity, and the S/L_y ratio. The heat flux from the plasma to the surface Q_p depends on the density at the sheath entrance n_s, the ionic T_i and electronic T_e temperatures, as well as the recombination energy for hydrogen E_i and the work function B_w. It writes [15]:

$$Q_p = \frac{J_i}{e}\left(2k_bT_i + e\phi_s + E_i - B_w\right) + \frac{J_{es}}{e}\left(2k_bT_e + B_w\right), \tag{2}$$

where $J_i = en_sc_s$ is the ion current and $J_{es} = \frac{en_sc_e}{4}\exp\left(-\frac{e\phi_s}{k_bT_e}\right)$ is the electron one; c_s is the ion acoustic velocity and $c_e = \sqrt{\frac{8k_bT_e}{\pi m}}$ where m is the electron mass and ϕ_s is the electric potential at the sheath entrance (which is positive with respect to the grounded left wall).

The heat flux Q_c from the surface in our model is attributed to conduction through the wall, radiation, and the heat flux carried by thermionic electrons penetrating the plasma. It writes:

$$Q_c = \frac{\kappa}{l}\left(T_s - T_0\right) + \epsilon\sigma T_s^4 + \frac{J_s(T_s)}{e}\left(B_w + 2k_bT_s\right), \tag{3}$$

where ϵ is the emissivity of the surface and σ is the Stefan–Boltzmann constant.

To determine the potential at the sheath entrance ϕ_s, which affects both heat fluxes, it is necessary to balance the charges at the wall so that the total current is zero and quasi-neutrality is maintained. According to the notations in Fig. 1, we can write that:

$$L_yJ_i + SJ_s = SJ_{es} + (L_y - S)J_e. \tag{4}$$

Assuming the electron flux at the spot is very close to that reaching the surrounding surface, $J_{es} \simeq J_e$, to reduce the system's dimensionality, we have $J_i + S/L_y \times J_s \simeq J_e$. This allows us to calculate ϕ_s as (see Ref. [21]):

$$e\phi_s = e\phi_f - k_bT_e\log\left(1 + \frac{S}{L_y}\frac{J_s}{en_sc_s}\right), \tag{5}$$

where ϕ_f is the well-known floating wall potential given by $-\frac{k_bT_e}{2e}\log\left(2\pi\frac{m}{M}(1+\frac{T_i}{T_e})\right)$; M is the considered ion mass (hydrogen). In the following we will assume that $n_s = \frac{1}{2}n_0$, with n_0 the plasma density. Note that the ambipolarity condition given by Eq. (4) does not allow for the direct use of this model in the case of thermionic current emitted at the mono-blocks during macroscopic melting events where there should be a net current integrated over L_y (if L_y is the sample size).

The surface temperature T_s for given plasma conditions can thus be calculated by finding the intersection of the $Q_p(T_s)$ and $Q_c(T_s)$ curves: by fixing T_s, we can calculate the current J_s and so the sheath potential ϕ_s using expression (5), leading to the determination of the two heat fluxes through Eqs. (2) and (3). An additional condition is necessary in calculating T_s because the sheath potential cannot decrease to zero as explained earlier and one needs to evaluate the electric field at the surface E_s and determine the critical temperature at which it cancels in order to get J_s^*. Note that the present case can only be rigorously treated in two dimensions, accounting for potential variations around the spot in both x and y directions. However, as we did above to calculate currents at the surface to derive Eq. (5), we can rely on a one dimensional case to determine the critical couple (J_s^*, ϕ_s^*) at which $E_s(J_s^*, \phi_s^*) = 0$. Therefore as we did in our previous study [21], we used here the expression of E_s derived by Hobbs and Wesson in their model [13]. We thus neglect the motion of electrons in the y-direction and assume that they accumulate in front of the spot as in a one-dimensional case.

In Fig. 2a are depicted the variations of the heat fluxes Q_p and Q_c with respect to T_s calculated with Eqs. (2) and (3) for a hydrogen plasma with $k_bT_i = k_bT_e = 35$ eV, $n_0 = 0.2 \times 10^{19}$ $\mathrm{m^{-3}}$ and $\kappa = 15$ $\mathrm{Wm^{-1}K^{-1}}$. The general trend of these flux curves, particularly of Q_p, can be explained by the relative weight of the thermionic current in Eq. (5), which gives the sheath potential. This weight is monitored by the ratio Ly/S: the larger it is, the closer ϕ_s is to ϕ_f, and the heat flux deposited by the electrons on the surface decreases. Similarly, a larger

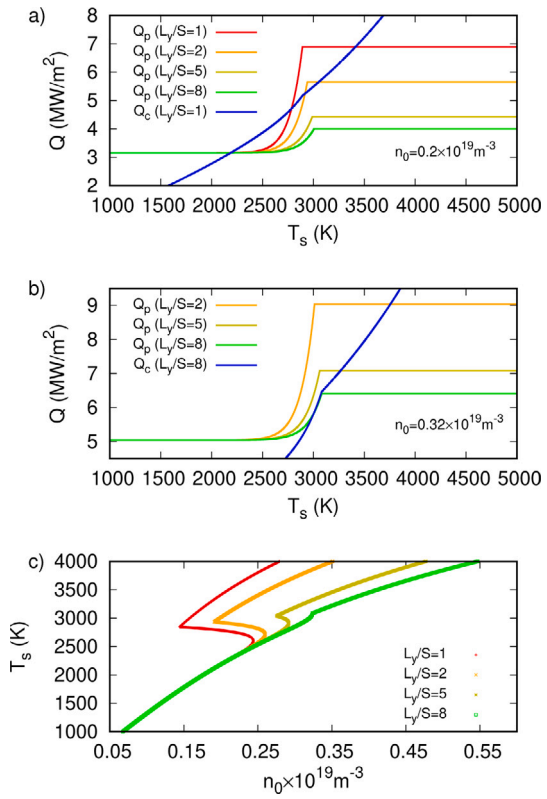

Fig. 2. (a) Heat flux from the plasma Q_p for different L_y/S ratios and for a plasma density $n_0 = 0.2 \times 10^{19}$ m^{-3}. Q_c is the heat flux from the surface. (b) Q_p and Q_c for a plasma density $n_0 = 0.32 \times 10^{19}$ m^{-3}. (c) Spot temperature T_s with respect to the plasma density n_0 for different L_y/S ratios. In all simulations, $k_bT_i = k_bT_e = 35$ eV.

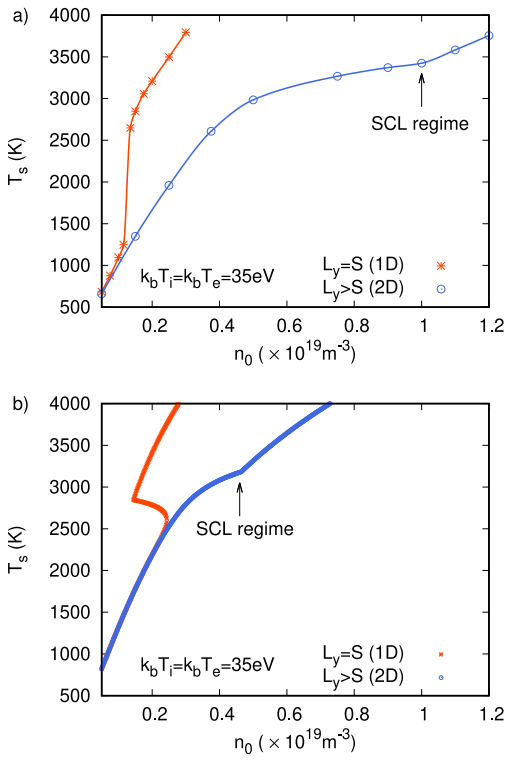

Fig. 3. (a) Variation of the spot temperature T_s for attached-like divertor conditions with respect to the plasma density n_0 calculated thanks to PIC simulations. (b) Spot temperature determined by fluid modeling as presented in Section 2.

current J_s can be emitted by the spot before reaching the SCL regime, where Q_p no longer varies with T_s (ϕ_s remaining equal to ϕ_s^* over this temperature range). The intersection of the characteristics $Q_p = Q_c$ further shows that for this specific density, there is a bifurcation in the cases $L_y/S = 1$ and $L_y/S = 2$. This type of bifurcation has already been identified numerically and experimentally by several authors [15, 22]. Although three distinct solutions are found (two stable and one metastable), the system will tend to transition abruptly between the two stable solutions, meaning it will shift from a regime of low thermo-emission to a highly emissive regime and reciprocally when plasma density is slightly changed.

When the plasma density increases as in Fig. 2b, the heat flux curves Q_p are shifted upward. Where a bifurcation appeared, for example, for $L_y/S = 2$ and $n_0 = 0.2 \times 10^{18}$ m^{-3}, the intersection $Q_p = Q_c$ shows here that the system has transitioned to the high-temperature regime, corresponding to a region of strong thermionic emission. More surprisingly, the bifurcation disappears for high ratios $L_y/S > 8$: the slope of the $Q_c(T)$ curve becomes steeper than that of $Q_p(T)$, and only one intersection point is found in the region of interest, i.e., in the range 2500–3000 K. The variations of T_s with plasma density extracted from these types of characteristics are shown in Fig. 2c. Generally, it can be noted that:

- In the regime where the spot emits little or no current J_s ($T_s <$ 2500 K), the impact of the Ly/S ratio is marginal, and the spot temperature varies similarly with n_0. It is indeed the plasma density that drives the behavior of the spot because other parameters (Ti, Te, or ϕ_s) are unchanged.
- The spot temperature at which the bifurcation occurs when traversing the curve from ascending or descending densities increases with the L_y/S ratio because the latter reduces the weight of J_s in expression (5). Finally, for the same plasma density, in the SCL regime, the spot temperature is lower when the L_y/S ratio increases, giving a larger area for the return of the plasma electron current to the surface.

3. PIC simulations

PIC simulations were used to verify if the 1D approximation from the previous section remains valid for determining the surface temperature of an isolated spot. The simulated system is similar to that presented in Fig. 1. At each iteration, the heat flux from the plasma deposited on the spot is calculated, and T_s is determined by equating this flux with Q_c given by Eq. (3). This allows for the injection of a specific number of thermionic electrons at the same iteration using the Richardson formula [Eq. (1)]. This procedure is repeated as long as necessary to reach a steady state. For more details on our numerical model, interested readers may consult Ref. [21].

We specifically studied two plasma conditions corresponding to attached or detached divertor plasma with typical temperatures of $k_bT_i = k_bT_e = 35$ eV and $k_bT_i = k_bT_e = 5$ eV, respectively. The plasma density n_0 was varied in both cases over the range 10^{18} - 10^{20} m^{-3} to calculate the evolution of the spot temperature and eventually reach the SCL regime. Its maximum value for attached divertor conditions is 1.2×10^{19} m^{-3} and 16×10^{19} m^{-3} for detached ones. The thermal conductivity of the spot was kept constant to 15 Wm^{-1}K^{-1}. Note that to facilitate scaling with plasma density in the PIC simulations and maintain a constant number of cells in the x direction, the size L_x

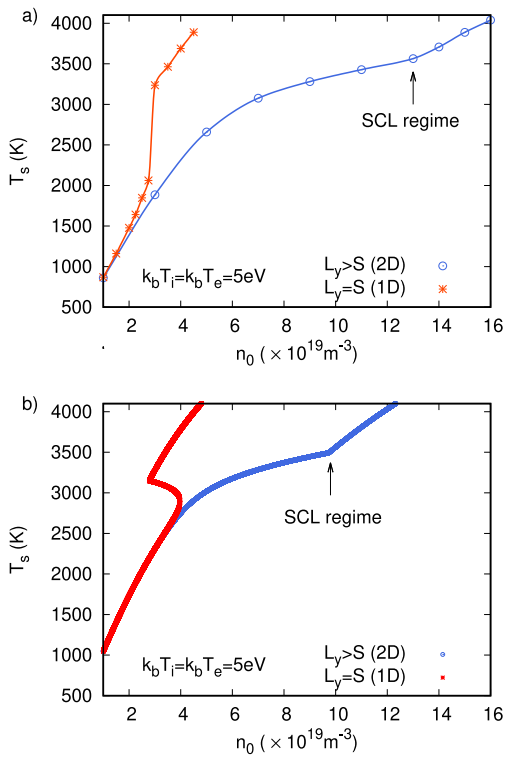

Fig. 4. (a) Variation of the spot temperature T_s for detached-like divertor conditions with respect to the plasma density n_0 calculated thanks to PIC simulations. (b) Spot temperature determined by fluid modeling as presented in Section 2.

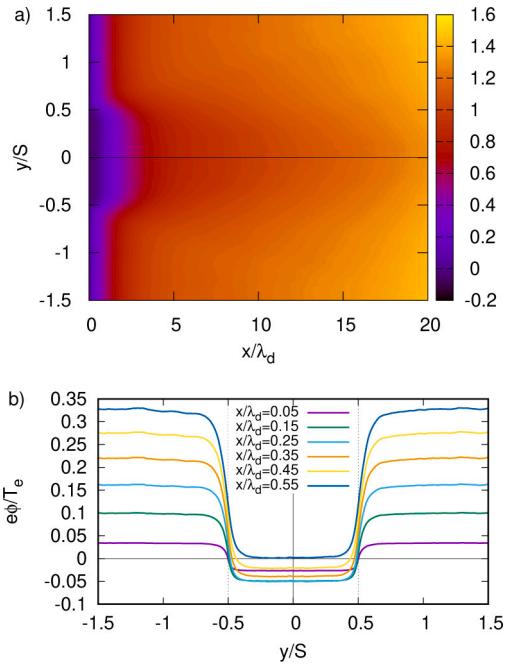

Fig. 5. (a) Zoom of the 2D density plot of the plasma potential normalized to T_e in the detached-plasma case for $n_0 = 15 \times 10^{19}$ m^{-3}. (b) Corresponding variation of the normalized potential in the y direction for different abscissas exhibiting the virtual cathode at the spot location.

is fixed at $50\lambda_d$. This is small compared to what is usually used in PIC simulations, but in the absence of magnetic field and with a thin sheath, is large enough to capture the physics of the system. When the entire surface emits thermionic electrons, i.e., $L_y = S$, the simulations are conducted using a 1D PIC code as in our previous study [21] and corresponding results labeled $L_y = S$ in the following. When current feedback is possible through the area surrounding the spot with $L_y > S$ (with a fixed $S = 20$ μm), then L_y is set to $50\lambda_d$ for the same reasons as previously mentioned for L_x and the use of a 2D PIC code is mandatory. The latter results are labeled $L_y > S$ in the text and in the figures.

In Fig. 3 is displayed the temperature variation of the spot with respect to the plasma density for attached-like divertor conditions obtained with the PIC code (a) and compared to that calculated with the fluid approach detailed in Section 2, (b). The same comparison for a detached-like divertor plasma is depicted in Fig. 4.

In both simulated plasma conditions and for both approaches (PIC vs fluid), the same trend is observed, namely the disappearance of the bifurcation (the rapid jump of T_s at a critical density) when $L_y > S$, with a smooth variation of T_s vs n_0 until the SCL is reached. Then a change in the slope marks the entry into the latter and the spot temperature increases more rapidly. A typical 2D potential profile corresponding to this regime is shown in Fig. 5 with a virtual cathode at the spot vicinity regulating the thermionic emission. Note that as the Debye length decreases with n_0, it turns out $L_y/S > 30$ and 3 in both attached and detached cases (see Fig. 6). Furthermore, the spot temperature is always higher when $L_y/S = 1$ in the SCL regime but is equivalent to the case $L_y > S$ for lower densities, as predicted by the fluid modeling. Although PIC results do not exhibit the typical "S" curve of the fluid approach and the associated hysteresis, they are in relative good agreement. We evidenced such hysteresis in our previous PIC study by managing the time delay at which thermionic electrons were injected into the system [21] (after or before the sheath building), but did not reproduce this approach here. Finally, the fluid modeling does not allow for precise determination of the entry into the SCL regime when $L_y/S > 1$, which is certainly due to the 1D approximation made for the calculation of the sheath potential.

Concerning the thermionic current penetrating into the plasma, its amplitude is directly correlated to the ratio L_y/S as depicted in Fig. 6. When $L_y/S = 1$, J_s increases from almost zero to its maximal value J_s^*, which is 2.9 and $3.5en_0c_s$ for the attached and detached divertor case respectively, at the bifurcation threshold. When ambipolarity is preserved due to the return of the electron current around the spot, in the region of size $L_y - S$, as explained by Eq. (4), it is possible to significantly increase the current J_s^*, i.e., the surface temperature before the apparition of the SCL regime. For a typical attached divertor plasma, J_s/n_0c_s saturates at 12.9 around 3420 K and at 6 at a temperature of 3700 K in the case of a detached divertor plasma; both values are quite larger to what is evidenced for $L_y/S = 1$.

4. Conclusion

In this paper, we have investigated the thermal behavior of a localized spot over a tungsten surface under the thermal load of a hot plasma whose density was varied. Our calculations show that if the entire surface emits electrons ($L_y = S$), then a bifurcation regime appears for a critical heat flux (which itself depends on the plasma temperature and its density). During this bifurcation, the sheath potential decreases abruptly to its minimum and the space-charge-limited regime appears: the surface temperature increases rapidly with a maximum current. Now, if we consider a thermally isolated spot on a surface with reduced conductivity, the bifurcation regime disappears ($L_y > S$). The surface temperature then increases continuously with the plasma density until it reaches the limited regime, and then continues to increase with a different slope. The maximum current density emitted by the spot in this case is much higher because there is a possibility for the electron current to circulate between the surface surrounding the spot and the plasma, as in the unipolar arc model.

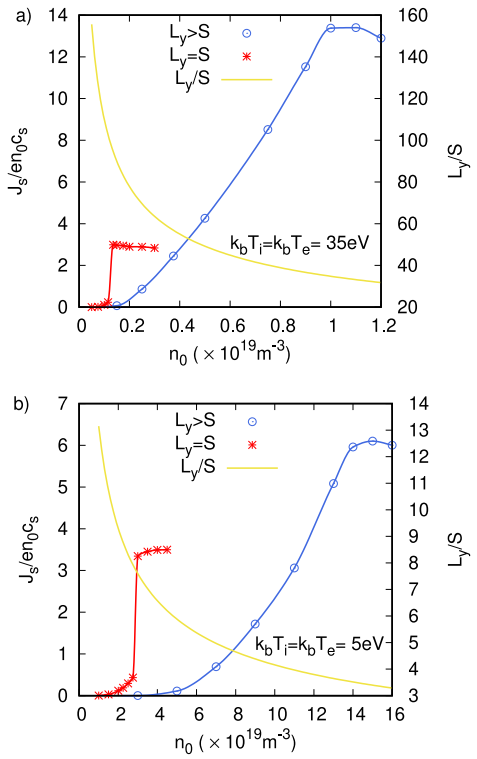

Fig. 6. Variation of the thermionic current density J_s for (a) attached-like and (b) detached-like divertor plasma conditions and for the case $L_y = S$ and $L_y = 50\lambda_d > S$. The ratio L_y/S plotted in yellow is indicative of the surface available for the return of the plasma electron current in order to achieve quasi-neutrality. (For interpretation of the references to color in this figure legend, the reader is referred to the web version of this article.)

CRediT authorship contribution statement

J. Moritz: Writing – original draft, Software, Resources, Formal analysis, Conceptualization. **S. Heuraux:** Writing – review & editing, Formal analysis. **M. Lesur:** Writing – review & editing, Software. **E. Gravier:** Writing – review & editing, Formal analysis. **F. Brochard:** Writing – review & editing, Resources. **L. Marot:** Writing – review & editing, Resources. **P. Hiret:** Writing – review & editing, Formal analysis.

Declaration of competing interest

The authors declare that they have no known competing financial interests or personal relationships that could have appeared to influence the work reported in this paper.

Data availability

Data will be made available on request.

Acknowledgments

This work was supported by the French National Research Agency (Agence Nationale de la Recherche) under project SHEAR ANR-19-CE30-033-01. It has been also carried out within the framework of the EUROfusion Consortium, funded by the European Union via the Euratom Research and Training Programme (Grant Agreement No 101052200 — EUROfusion). Views and opinions expressed are however those of the author(s) only and do not necessarily reflect those of the European Union or the European Commission. Neither the European Union nor the European Commission can be held responsible for them.

References

[1] V. Bobkov, D. Aguiam, R. Bilato, et al., Impact of ICRF on the scrape-off layer and on plasma wall interactions: From present experiments to fusion reactor, Nucl. Mater. Energy 18 (2019) 131.
[2] J. Coenen, G. Arnoux, B. Bazylev, et al., ELM-induced transient tungsten melting in the JET divertor, Nucl. Fusion 55 (2015) 023010.
[3] Y. Corre, A. Grosjean, J.P. Gunn, et al., Sustained W-melting experiments on actively cooled ITER-like plasma facing unit in WEST, Phys. Scr. 96 (2021) 124057.
[4] K. Krieger, M. Balden, J. Coenen, et al., Experiments on transient melting of tungsten by ELMs in ASDEX upgrade, Nucl. Fusion 58 (2018) 026024.
[5] M. Komm, S. Ratynskaia, P. Tolias, A. Podolnik, Space-charge limited thermionic sheaths in magnetized fusion plasmas., Nucl. Fusion 60 (2020) 054002.
[6] M. Komm, S. Ratynskaia, P. Tolias, et al., On thermionic emission from plasma-facing components in tokamak-relevant conditions, Plasma Phys. Control. Fusion 59 (2017) 094002.
[7] P. Tolias, M. Komm, S. Ratynskaia, A. Podolnik, ITER relevant multi-emissive sheaths at normal magnetic field inclination, Nucl. Fusion 63 (2023) 026007.
[8] E. Thorén, S. Ratynskaia, P. Tolias, et al., The MEMOS-U code description of macroscopic melt dynamics in fusion devices, Plasma Phys. Control. Fusion 63 (2021) 035021.
[9] S. Ratynskaia, E. Thorén, P. Tolias, et al., The MEMOS-U macroscopic melt dynamics code benchmarking and applications, Phys. Scr. 96 (2021) 124009.
[10] S.A. Barengolts, G.A. Mesyats, M.M. Tsventoukh, The ecton mechanism of unipolar arcing in magnetic confinement fusion devices, Nucl. Fusion 50 (2010) 125004.
[11] V. Rohde, M. Balden, R. Neu, Arc behaviour on different materials in ASDEX-Upgrade, Nucl. Mater. Energy 29 (2021) 101083.
[12] B. Wang, D. Zhu, R. Ding, et al., Observations on arcing on the metal plasma-facing components in EAST, Nucl. Mater. Energy 34 (2023) 101318.
[13] G.D. Hobbs, J.A. Wesson, Heat flow through a langmuir sheath in the presence of electron emission, Plasma Phys. 9 (1967) 85.
[14] C. Herring, M.H. Nichols, Thermionic emission, Rev. Modern Phys. 21 (1949) 185.
[15] M. Tokar, A. Nedospasov, A. Yarochkin, The possible nature of hot spots on tokamak walls, Nucl. Fusion 32 (1992) 15.
[16] R.D. Smirnov, A.Y. Pigarov, M. Rosenberg, S.I. Krasheninnikov, D.A. Mendis, Modelling of dynamics and transport of carbon dust particles in tokamaks, Plasma Phys. Control. Fusion 49 (2007) 347.
[17] A.E. Robson, P.C. Thonemann, An arc maintained on an isolated metal plate exposed to a plasma, Proc. Phys. Soc. 73 (1959) 508.

[18] F.R. Schwirzke, Vacuum breakdown on metal surfaces, IEEE Trans. Plasma Sci. 19 (1991) 690.
[19] S. Cui, M. Simmonds, W. Qin, et al., Thermal conductivity reduction of tungsten plasma facing material due to helium plasma irradiation in PISCES using the improved 3-omega method, J. Nucl. Mater. 486 (2017) 267.
[20] S. Ratynskaia, P. Tolias, M.D. Angeli, et al., Interaction of metal dust adhered on castellated substrates with the ELMy H-mode plasmas of ASDEX-Upgrade, Nucl. Fusion 58 (2018) 106023.
[21] J. Moritz, S. Heuraux, N. Lemoine, et al., Thermionic emission of a tungsten surface in high heat flux plasma: PIC simulations, Phys. Plasmas 30 (2023) 083514.
[22] M.Y. Ye, S. Takamura, N. Ohno, Study of hot tungsten emissive plate in high heat flux plasma on NAGDIS-I, J. Nucl. Mater. 241 (1997) 1243.